Molecular Cell
Article

Conserved Antagonism between JMJD2A/KDM4A and HP1γ during Cell Cycle Progression

Joshua C. Black,[1] Andrew Allen,[1,5] Capucine Van Rechem,[1,5] Emily Forbes,[1,5] Michelle Longworth,[1] Katrin Tschöp,[1] Claire Rinehart,[2] Jonathan Quiton,[3] Ryan Walsh,[1] Andrea Smallwood,[4] Nicholas J. Dyson,[1] and Johnathan R. Whetstine[1,*]
[1]Massachusetts General Hospital Cancer Center and Department of Medicine, Harvard Medical School, 13th Street, Charlestown, MA 02129, USA
[2]Department of Biology
[3]Department of Mathematics and Computer Science
Western Kentucky University, 1906 College Heights Boulevard, Bowling Green, KY 42101-1078, USA
[4]Ludwig Institute for Cancer Research UCSD, 9500 Gilman Drive, La Jolla, CA 92093, USA
[5]These authors contributed equally to this work
*Correspondence: jwhetstine@hms.harvard.edu
DOI 10.1016/j.molcel.2010.11.008

SUMMARY

The KDM4/JMJD2 family of histone demethylases is amplified in human cancers. However, little is known about their physiologic or tumorigenic roles. We have identified a conserved and unappreciated role for the JMJD2A/KDM4A H3K9/36 tridemethylase in cell cycle progression. We demonstrate that JMJD2A protein levels are regulated in a cell cycle-dependent manner and that JMJD2A overexpression increased chromatin accessibility, S phase progression, and altered replication timing of specific genomic loci. These phenotypes depended on JMJD2A enzymatic activity. Strikingly, depletion of the only *C. elegans* homolog, JMJD-2, slowed DNA replication and increased ATR/p53-dependent apoptosis. Importantly, overexpression of HP1γ antagonized JMJD2A-dependent progression through S phase, and depletion of HPL-2 rescued the DNA replication-related phenotypes in *jmjd-2*$^{-/-}$ animals. Our findings describe a highly conserved model whereby JMJD2A regulates DNA replication by antagonizing HP1γ and controlling chromatin accessibility.

INTRODUCTION

In eukaryotes, DNA is packed into a highly ordered chromatin structure composed of DNA, histones, and other chromosomal proteins. Posttranslational modification (PTM) of histones plays an instrumental role in integrating extra- and intracellular signals to regulate DNA-dependent processes. The dynamics associated with histone PTMs are critical determinants of stem cell fate and maintenance, tissue patterning, and the inhibition of tumor growth (Bernstein et al., 2007; Fraga and Esteller, 2005; Moss and Wallrath, 2007). Multiple lysine (K) residues on the tails of histone H3 and H4 have been shown to be sites for methylation. The site and degree of methylation (mono-, di-, or tri-) are critical for heterochromatin formation and maintenance, replication timing, and gene expression (Chen et al., 2008; Grewal and Jia, 2007; Maison et al., 2002; Wu et al., 2005). Moreover, aberrant methylation can result in human diseases such as cancer (Fraga and Esteller, 2005; Moss and Wallrath, 2007).

The FAD-dependent amine oxidases and the JmjC-containing histone demethylases regulate methylation balance with specificity for particular lysines, and for the degree of methylation (Cloos et al., 2008; Klose et al., 2006; Lan et al., 2008; Whetstine et al., 2006). For example, the JMJD2/KDM4 family demethylates trimethylated H3K9, H3K36, and H1.4K26 (Fodor et al., 2006; Klose et al., 2006; Trojer et al., 2009; Whetstine et al., 2006). There are four JMJD2 family members in humans, JMJD2A-D, and one in *C. elegans*, JMJD-2 (Whetstine et al., 2006). We previously demonstrated that the depletion of JMJD-2 increased DNA double-strand breaks (DSBs) in the adult germline, which resulted in p53-dependent apoptosis (Whetstine et al., 2006). These observations underscore the importance of balancing methylation levels so that DNA damage and p53-dependent apoptosis are avoided.

At least part of the function of histone methylation is mediated through recruitment of Heterochromatin Protein 1 (HP1) family members. There are three mammalian HP1 proteins, HP1α, HP1β, and HP1γ, which are recruited to H3K9me3 and H1.4K26me3 (Bannister et al., 2001; Daujat et al., 2005; Lachner et al., 2001; Trojer et al., 2009). While HP1α and HP1β are generally localized to heterochromatin, HP1γ is present in both heterochromatic and euchromatic domains (Kwon and Workman, 2008; Vakoc et al., 2005).

Emerging evidence suggests HP1 proteins are important regulators of DNA replication, which is exemplified through regulation of pericentric heterochromatin. Pericentric heterochromatin is the region that surrounds the centromere and is highly condensed and H3K9me3 enriched (Chen et al., 2008; Grewal and Jia, 2007; Weidtkamp-Peters et al., 2006; Wu et al., 2005). Deletions of the yeast H3K9me3 methyltransferase (CLR4) and SWI6 (yeast HP1 homolog) result in altered S phase progression and replication stress (Biswas et al., 2008; Grewal and Jia, 2007; Kim et al., 2008). Additionally, SWI6 localizes to pericentric regions and heterochromatin foci in a Chromatin Assembly

Factor-1 (CAF-1, a chaperone important for histone assembly during replication)-dependent manner (Dohke et al., 2008). SWI6 is also required for proper replication timing of pericentric heterochromatin in fission yeast (Hayashi et al., 2009).

Similarly, in mammalian cells, HP1α, HP1β, and H3K9me3 are important for condensing pericentric regions to maintain transcriptional repression and to prevent this region from being aberrantly replicated (Bannister et al., 2001; Czvitkovich et al., 2001; Nakayama et al., 2001; Quivy et al., 2008). Mammalian HP1α and HP1γ also directly interact with components of the replication fork, including CAF-1 (Huang et al., 1998; Quivy et al., 2008). The HP1α and CAF-1 association is critical for maintaining the late replication of pericentric heterochromatin during S phase (Quivy et al., 2008). Interestingly, no role has been ascribed to HP1γ in DNA replication.

Heterochromatin and H3K9me3-enriched regions tend to replicate late during S phase (e.g., satellites), which has been confirmed by genome-wide and locus-specific analyses (Mendez, 2009). Additional studies have further demonstrated that chromatin accessibility is a critical determinant of DNA replication timing (Hansen et al., 2010; Karnani et al., 2010; MacAlpine et al., 2004, 2010). For example, active gene expression and DNase I hypersensitivity are associated with earlier DNA replication. However, active transcription is not required to replicate earlier as altering histone acetylation at specific loci changes replication timing without altering transcription (Cimbora et al., 2000; Schubeler et al., 2000). These observations strongly suggest that an open chromatin configuration is a strong indicator of whether a region will replicate in early or late S phase.

In this study, we demonstrate that the histone tridemethylase JMJD2A regulates cell cycle progression by increasing chromatin accessibility and antagonizing HP1γ occupancy. Overexpression of catalytically active JMJD2A resulted in faster S phase progression, corresponding to a more open chromatin state, increased single-strand DNA (ssDNA) generation, increased BrdU incorporation, and loss of HP1γ at target loci. Strikingly, HP1γ overexpression, but not HP1α or HP1β, abrogated JMJD2A-dependent replication changes at both a cellular and locus-specific level. Antagonism by HP1γ was dependent on both the chromodomain and the chromo shadow domain. Consistent with our observations in human cell culture, loss of JMJD-2 in *C. elegans* results in increased DNA damage, slower DNA replication, and ATR/p53-dependent apoptosis. Furthermore, the loss of the *C. elegans* HP1 homolog HPL-2 rescued the increased DNA damage, the impaired DNA replication, and the ATR/p53-dependent apoptosis observed upon JMJD-2 depletion. Taken together, the data in both human cell culture and *C. elegans* demonstrate a highly conserved and unappreciated role for JMJD2A/JMJD-2 in DNA replication and S phase progression by altering chromatin accessibility and antagonizing HP1γ/HPL-2.

RESULTS

JMJD2A Protein Levels Are Regulated over Cell Cycle

To determine if JMJD2A/KDM4A was regulated throughout the cell cycle, we immunoblotted whole-cell extracts from asynchronous cells, cells synchronized at G1/S and S with hydroxyurea (HU) arrest and release and cells in G2/M (nocodazole arrest) (Figure 1A). Flow cytometry confirmed the cell cycle profiles (see Figures S1A and S1B available online). JMJD2A peaked during G1/S with a decrease during S phase reaching the lowest levels during G2/M (Figure 1A). JMJD2A transcript levels remained comparable over the cell cycle (Figures S1C and S1D), which suggests JMJD2A protein levels are posttranscriptionally regulated. JMJD2A expression was similar following nocodazole release (peaking after 6–7 hr, G1/S), demonstrating that HU-related DNA damage did not result in the JMJD2A protein changes (Figure 1B).

JMJD2A Overexpression Alters Cell Cycle Progression

We ectopically expressed JMJD2A to determine its effect on cell cycle progression (Figure 1B). We created stable HEK293T cells expressing control, JMJD2A, or catalytically inactive JMJD2A^{H188A} (Whetstine et al., 2006). These cell lines exhibited modest 2- to 3-fold overexpression of both JMJD2A and JMJD2A^{H188A} (Figure 1B and Figure S1E) that did not result in decreased global levels of H1.4K26me3 or H3K9/36me3 (Figure S1F). Interestingly, ectopic expression of JMJD2A resulted in stabilization of both endogenous and exogenous JMJD2A throughout the cell cycle (Figure 1B). JMJD2A overexpression, but not JMJD2A^{H188A}, resulted in faster S phase progression (Figure 1C; note red arrow at 10 and 12 hr postnocodazole). A graphical representation of the average percentage of cells reaching late S phase is shown in Figure 1D.

To gain insight into JMJD2A-dependent faster S phase progression, we analyzed the amount of ssDNA generated following release from nocodazole, which indicates if additional replication forks are present (Jasencakova et al., 2010). At 6 and 10 hr postnocodazole release, we observed an increase in ssDNA in JMJD2A but not JMJD2A^{H188A} overexpressing cells (Figures 1E and 1F). These data are consistent with an increase in replication forks in JMJD2A cells, which promote faster S phase progression, at least in part, by increasing replication initiation.

We further tested the relationship between JMJD2A and DNA replication by conducting BrdU immunoprecipitations of specific genomic loci in asynchronous cells. JMJD2A overexpression, but not JMJD2A^{H188A}, resulted in increased BrdU incorporation at chromosome 1 satellite 2 (Chr1 sat2), a region enriched for H3K9me3 and HP1γ (Hansen et al., 2010; Zeng et al., 2009) (Figure 1G, $p = 0.0218$). Similar results were obtained with a region near the X centromere (designated X cen, Figure S1G). In contrast, an ALU repeat on chromosome 19 with minimal H3K9me3 was not regulated by JMJD2A (Figure S1H) (Zeng et al., 2009).

Since JMJD2A-overexpressing cells progressed through S phase faster, had increased replication forks, and increased BrdU incorporation at Chr1 sat2, we reasoned that JMJD2A could be impacting the timing of replication of specific regions. To determine if JMJD2A altered replication timing, we sorted live cells labeled with BrdU by flow cytometry, collected multiple S phase fractions (Figure S1I), and conducted BrdU IPs. As predicted, ectopic expression of JMJD2A resulted in earlier replication of Chr1 sat2 (Figure 1H) without impacting the replication timing of the β-actin locus (Figure S1I).

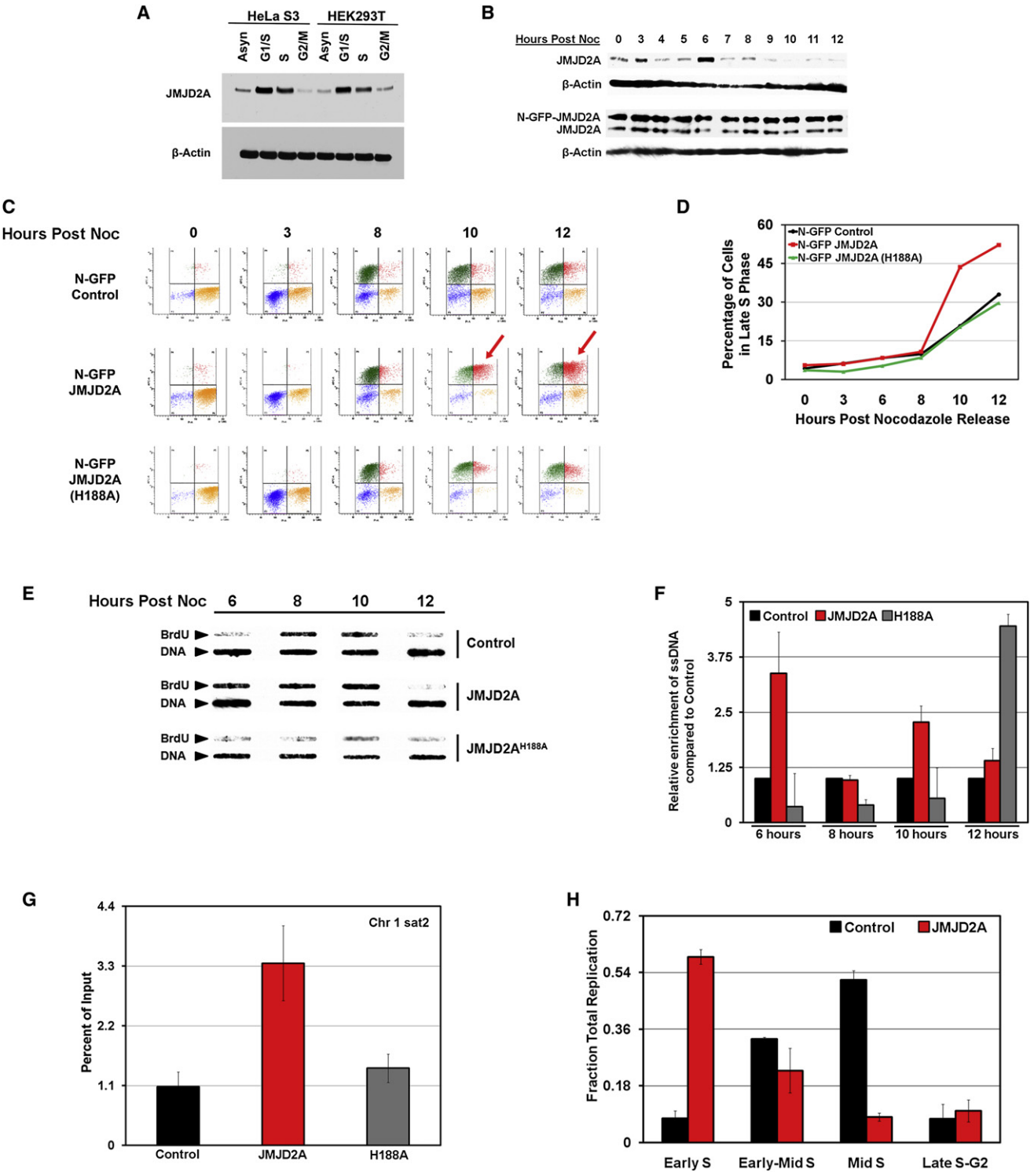

Figure 1. Overexpression of JMJD2A Allows Faster Progression through S Phase

(A) JMJD2A protein levels are regulated during cell cycle in whole-cell extracts from HU-arrested cells.

(B) JMJD2A protein levels are regulated during cell cycle in whole-cell extracts from nocodazole release.

(C) JMJD2A overexpression results in faster S phase progression using flow cytometry. The red arrow highlights the faster accumulation in late S phase.

(D) Graphical summary of the average percentage of control, JMJD2A, or catalytically inactive JMJD2A^{H188A} cells in late S phase.

(E) JMJD2A cells have increased ssDNA (indicative of replication forks) 6 and 10 hr post nocodazole release.

(F) Quantitation of (E). Error bars represent the SEM of biological replicates analyzed in duplicate.

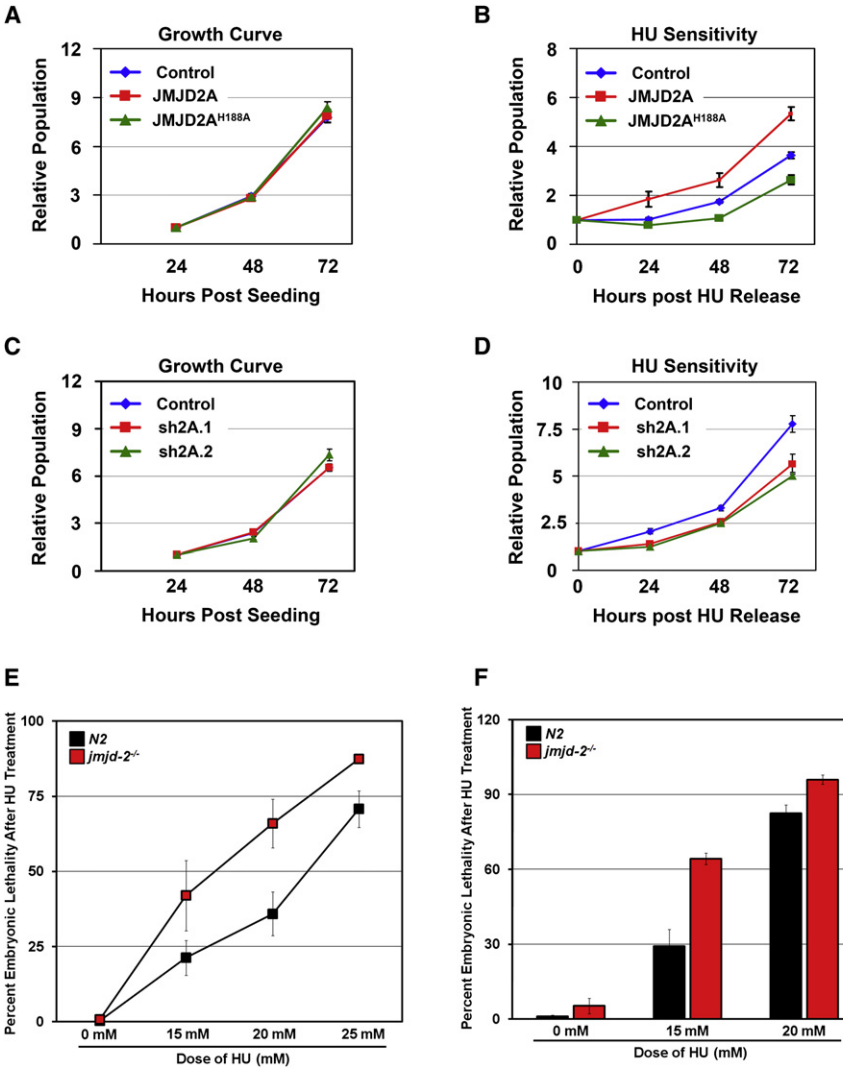

Figure 2. JMJD2A/JMJD-2 Expression Levels Alter Sensitivity to the Replication Inhibitor HU

(A) JMJD2A or JMJD2A^{H188A} cells do not have different growth rates compared to control cells.

(B) JMJD2A overexpression increases recovery from HU, while overexpression of catalytically inactive JMJD2A^{H188A} increases cell sensitivity to HU.

(C) Depletion of JMJD2A by two different shRNAs does not alter cell growth rates.

(D) Depletion of JMJD2A by two different shRNAs increases cellular sensitivity to HU. For (A)–(D), error bars represent the SEM of nine points from at least three biological replicates.

(E and F) When compared to wild-type N2 worms, *jmjd-2*$^{-/-}$ and *jmjd-2 (RNAi)*-treated worms show an increased embryonic lethality in response to HU. These experiments were conducted at least three independent times with at least 15 worms per genotype per experiment. Error bars represent the SEM.

JMJD2A Levels Impact the Cellular Response to Replication Stress

Factors involved in DNA replication often modulate response to replication stress (e.g., sensitivity to HU; Biswas et al., 2008; Kim et al., 2008). Therefore, we tested whether alterations in JMJD2A protein levels would affect the cellular response to HU. We treated control, JMJD2A-expressing, or JMJD2A^{H188A}-expressing cells with or without 1 mM HU for 24 hr before being released into fresh media (Figures 2A and 2B). Even though ectopic expression of JMJD2A leads to faster S phase progression, JMJD2A-overexpressing cells have similar growth curves when compared to control cells, suggesting that overexpressing cells have a delay in another part of the cell cycle (e.g., G2/M) (Figure 2A). However, ectopic expression of JMJD2A resulted in faster recovery from HU treatment (Figure 2B). Conversely, overexpression of catalytically inactive JMJD2A^{H188A} resulted in increased sensitivity to HU (Figure 2B). JMJD2A depletion with two different shRNA constructs also resulted in increased HU sensitivity with no change to standard growth (Figures 2C and 2D; expression levels shown in Figures S2A and S2B). Since JMJD2A depletion mimics the increased HU sensitivity of JMJD2A^{H188A} cells, we hypothesize that catalytically inactive JMJD2A acts as a dominant negative.

JMJD2 Proteins Impact DNA Replication in *C. elegans*

Since JMJD2A altered cell cycle progression, DNA replication, and sensitivity to DNA replication stress in human cells, we determined if these processes were regulated in vivo by evaluating the *jmjd-2(tm2966)* loss-of-function allele in *C. elegans* (referred to as *jmjd-2*$^{-/-}$). This allele has a 672 base pair deletion that is followed by an 18 base pair insertion, resulting in a frameshift that truncates the protein 25 amino acids into the JmjC domain, which eliminates enzymatic activity (Figure S3A).

(G) JMJD2A overexpression drives replication at chromosome 1 satellite 2 as measured using BrdU DNA IP. Error bars represent the SEM of four independent experiments. JMJD2A cells were statistically significantly different from control ($p = 0.0218$) while JMJD2A^{H188A} were not ($p = 0.4009$) using a two-tailed Student's t test.

(H) Overexpression of JMJD2A leads to earlier replication of Chr1 sat2 (compare control to JMJD2A cells: for early S, $p = 0.004$; for mid-S, $p = 0.005$). The graph shows the fraction of Chr1 sat2 replicated in each fraction compared to total across all fractions (BrdU incorporation of each fraction compared to input). Error bars represent the SEM.

We determined whether *jmjd-2*$^{-/-}$ or *jmjd-2 (RNAi)*-treated worms had increased sensitivity to replication stress like the JMJD2A-depleted cells. As expected, both the *jmjd-2*$^{-/-}$ and the *jmjd-2 (RNAi)*-treated worms were more sensitive than wild-type worms to a dose range of HU (Figures 2E and 2F).

Similar to the *jmjd-2 (RNAi)*, *jmjd-2*$^{-/-}$ worms also had increased H3K9me3 and H3K36me3 levels and increased meiotic DSBs as determined by the number of RAD-51 foci per nucleus in midpachytene nuclei (Figures S3B–S3D; Whetstine et al., 2006). We also observed an increase in the number of RAD-51 foci in the mitotic zone, which likely reflects stalled or collapsed replication forks (Figure 3A; Garcia-Muse and Boulton, 2005). The increased RAD-51 foci in the mitotic zone were accompanied by larger, morphologically distinct nuclei that were phenotypically similar to HU-treated nuclei (Figure S3E; Garcia-Muse and Boulton, 2005). These nuclei were greater than 4.2 microns in diameter, which is significantly larger than the 3.5 micron average of wild-type nuclei. Often, these HU-like nuclei had increased RAD-51 foci (Figures S3E and S3F). Furthermore, *jmjd-2*$^{-/-}$ worms had less nuclei in the mitotic zone when compared to wild-type worms (Figure 3B, 175 ± 3 nuclei versus 209 ± 2 nuclei, respectively; $p < 1 \times 10^{-15}$). The number of nuclear diameters between the distal tip cell and the transition zone was unchanged when compared to wild-type worms (20.4 ± 0.4 versus 20.8 ± 0.3, $p > 0.3$), suggesting impaired proliferation of a structurally normal mitotic zone.

To directly measure DNA replication in the *jmjd-2*$^{-/-}$ and wild-type adult *C. elegans* germline, we injected Cy3-dUTP and scored the number of nuclei that incorporated Cy3-dUTP in the first ten nuclear diameters. This region most likely reflects the germ cell nuclei in mitotic S phase (Figure S4A; Jaramillo-Lambert et al., 2007). The *jmjd-2*$^{-/-}$ worms had reduced Cy3-dUTP incorporation in the first ten nuclear diameters of the mitotic zone (Figures 3C and 3D and Figure S4B). The *jmjd-2*$^{-/-}$ worms consistently had more unlabeled nuclei when compared to wild-type worms (Figures 3C and 3D and Figure S4B). Using the same exposure settings, we also noted less overall signal per nucleus when compared to the wild-type worms.

Since decreased nucleotide incorporation could reflect less proliferation without impacting the timing of replication, we directly measured replication timing by utilizing a pulse-chase method in adult germlines (Jaramillo-Lambert et al., 2007). Cy3-dUTP was injected into adult germlines and after a 4 hour recovery Alexa 488-dUTP was injected into the same germline and allowed to incorporate for an additional hour. We then quantified the number of nuclei labeled with both Cy3- and Alexa 488-dUTP in each germline (designated dual labeled nuclei). At the same time, we scored the number of nuclei containing overlap of Cy3- and Alexa 488-dUTP incorporation at the same position within the chromosomes (yellow, designated colabeled nuclei). If replication is slower, there will be an increase in the number of germlines with dual labeled nuclei, as well as an increase in colabeled (yellow) chromosomal regions. We observed a significant increase in the number of germline nuclei that contained both Cy3-dUTP and Alexa 488-dUTP (Figures 3E and 3F), as well as colabeled regions within the same nucleus in *jmjd-2*$^{-/-}$ animals (Figures 3G and 3H). These results strongly indicate that JMJD-2 is required for the normal timing of DNA replication in vivo.

Similar to JMJD-2-depleted worms, *jmjd-2*$^{-/-}$ worms had increased germline apoptosis that was mediated by CEP-1 (the p53 homolog), which established a link to DNA damage-induced apoptosis (Figure 4A; Whetstine et al., 2006). Since loss of JMJD-2 slowed replication and increased damage, we reasoned that the increased apoptosis was a result of the replication stress kinase ATL-1 (the *C. elegans* ATR homolog) signaling to CEP-1. ATL-1 has been shown to act upstream of CEP-1 in *C. elegans* to trigger DNA damage-induced apoptosis (Stergiou et al., 2007). Consistently, ATL-1 depletion [*atl-1* (*tm853*) mutant or *atl-1*(*RNAi*); Garcia-Muse and Boulton, 2005] rescued the increased apoptosis observed in JMJD-2-depleted worms (Figure 4B). In contrast, the depletion of ATM-1 (PI3 kinase involved in DNA damage response to ionizing radiation) with either *atm-1 (RNAi)* or the *atm-1(gk186)* mutant worms did not provide a significant rescue (Figure 4C).

JMJD2A Overexpression Alters Chromatin Accessibility over Cell Cycle

Chromatin structure impacts DNA replication timing (Mendez, 2009). Since JMJD2A regulates histone methylation and has been shown to relocalize HP1 upon high levels of overexpression (Klose et al., 2006), we hypothesized that JMJD2A overexpression alters chromatin organization and DNA replication. If enough genomic regions are altered, we would observe modest changes in global chromatin structure. Therefore, we evaluated chromatin accessibility by micrococcal nuclease (MNase) digestion. Ectopic expression of JMJD2A, but not JMJD2A^{H188A}, produced a higher ratio of mononucleosomes to hexanucleosomes in asynchronous cells (Figure 5A). Quantitation of seven independent biological experiments revealed a modest but significant 1.9-fold increase in mononucleosomes following 15 min of MNase digestion (Figure 5B, $p = 0.032$).

We then evaluated chromatin accessibility during S phase. Control and JMJD2A-overexpressing cells were synchronized at G1/S with HU and nuclei were collected from arrested and released cells (2.5 and 5 hr) so that chromatin structure could be monitored over the course of S phase (Figure 5C). JMJD2A-overexpressing cells had more open chromatin in the G1/S-arrested cells and at each subsequent point through S phase (Figure 5C).

We hypothesized that JMJD2A alters the accessibility of specific genomic regions and in turn promotes DNA replication and S phase progression. To test this hypothesis, we examined the accessibility of Chr1 sat2 and X cen by Southern blot analysis of the MNase digests. We observed that sat2 was more accessible to MNase in asynchronous cells overexpressing JMJD2A (Figures 5D and 5E). X cen also exhibited an increase in chromatin accessibility, albeit more modest than sat2 (Figures S5A and S5B). Further, sat2 became more accessible during the progression of S phase in JMJD2A-overexpressing cells (Figure 5F). Interestingly, in JMJD2A-overexpressing cells, sat2 exhibited the strongest increase in accessibility 2.5 hr into S phase, which suggests this locus becomes more accessible earlier during S phase. These results demonstrate that the increased DNA replication observed at sat2 and X cen corresponds with

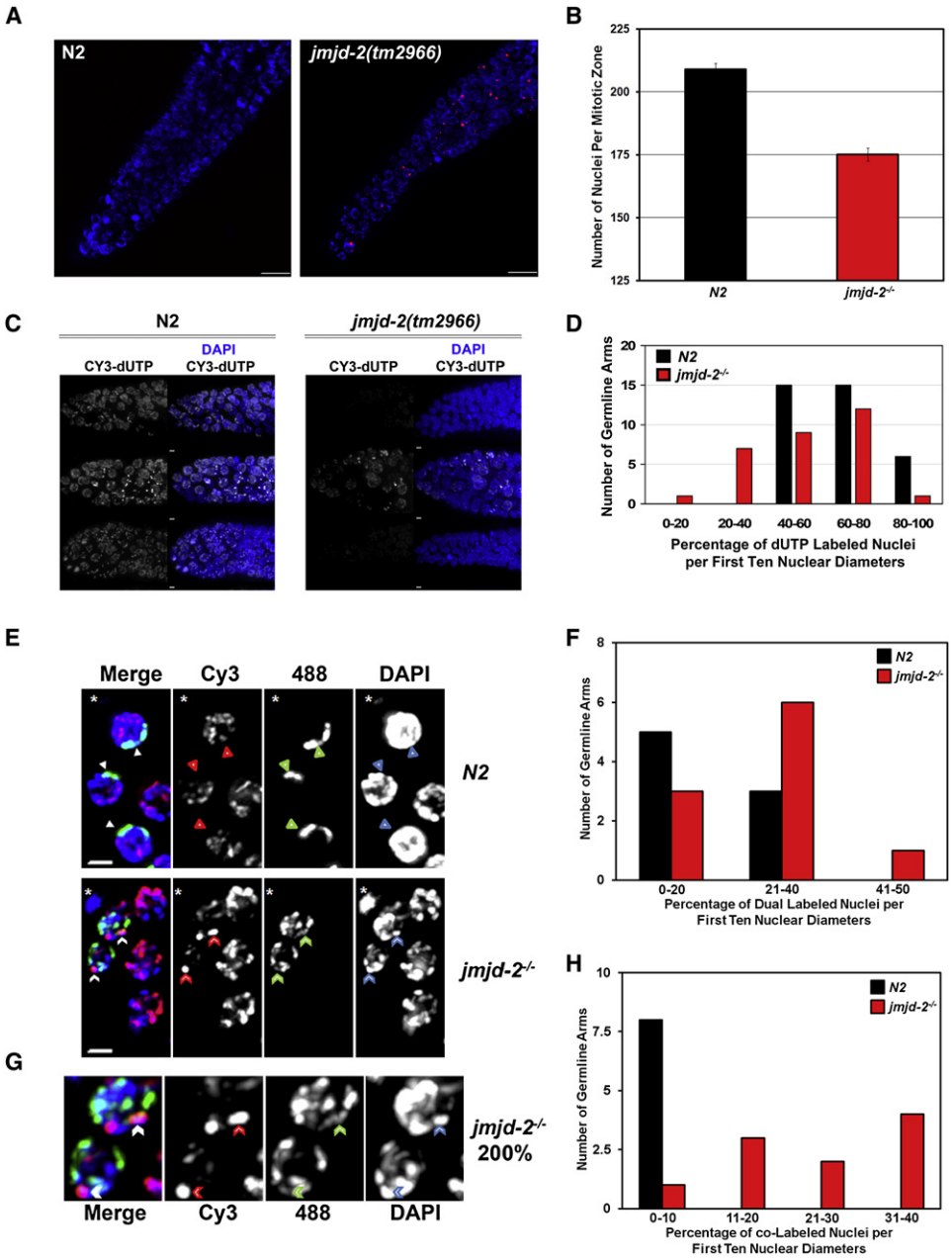

Figure 3. In Vivo Labeling of DNA Synthesis in Wild-Type and *jmjd-2*$^{-/-}$ Worms

(A) *jmjd-2*$^{-/-}$ worms have an increased frequency of RAD-51 foci within the mitotic zone. Scale bar, 10 μm.

(B) *jmjd-2*$^{-/-}$ mutants have a decreased number of nuclei in the mitotic zone. Error bars represent the SEM from scoring at least 30 germlines of each genotype ($p < 1 \times 10^{-15}$ by two-tailed Student's t test).

(C) *jmjd-2*$^{-/-}$ mutants have decreased replication in the mitotic zone as measured using Cy3-dUTP to label nuclei undergoing DNA replication. The first ten nuclear diameters of the mitotic zone are shown. The distal tip cell is on the left. A comprehensive panel of germlines scored is available in Figure S6. Cy3-dUTP is shown in white and DAPI is shown in blue. Scale bar, 2 μM.

(D) Quantitation of 36 wild-type and 30 *jmjd-2*$^{-/-}$ germlines scored blind for Cy3-dUTP incorporation.

(E) Representative nuclei from N2 or *jmjd-2*$^{-/-}$ worms double injected with Cy3-dUTP and 488-dUTP. Arrowheads indicate regions labeled with either Cy3- or 488-dUTP (dual labeled nuclei). Chevrons demonstrate chromosome regions labeled with both Cy3- and 488-dUTP (colabeled nuclei). Scale bar, 2 μM.

(F) Quantification of dual labeled nuclei.

(G) Magnified (200%) image of *jmjd-2*$^{-/-}$ nuclei from (E).

(H) Quantification of the colabeled nuclei in N2 and *jmjd-2*$^{-/-}$ worms.

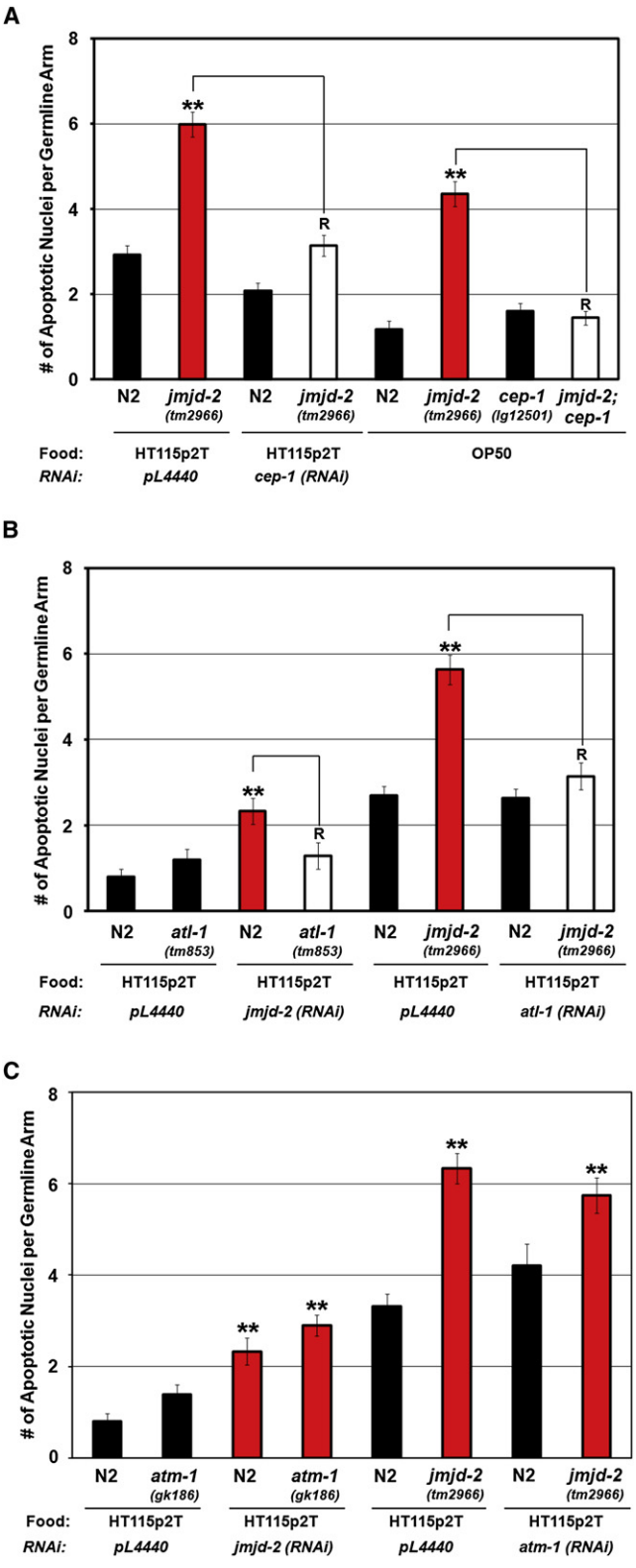

Figure 4. CEP-1 and ATL-1 Depletion Rescues the Increased DNA Damage-Based Apoptosis in JMJD-2-Depleted Worms

(A) CEP-1 depletion by either *cep-1 (RNAi)* or *cep-1(lg12501)* rescues the increased apoptosis observed in either *jmjd-2*$^{-/-}$ or *jmjd-2 (RNAi)*-treated worms.

(B) ATL-1 depletion by either *atl-1 (RNAi)* or *atl-1(tm853)* rescues the increased apoptosis observed in either *jmjd-2*$^{-/-}$ or *jmjd-2 (RNAi)*-treated worms.

(C) ATM-1 depletion by either *atm-1 (RNAi)* or *atm-1(gk186)* does not rescue the increased apoptosis observed in either *jmjd-2*$^{-/-}$ or *jmjd-2 (RNAi)*-treated worms. Each experiment was conducted at least three independent times with at least 30 germlines per genotype per experiment. The SEM is shown for each experiment. ** indicates $p < 0.0001$, and R indicates rescue and no significant difference from wild-type control by Student's t test ($p > 0.05$).

a more open chromatin environment (Figures 1G and 1H and Figure S1G).

HP1γ/HPL-2 Antagonize JMJD2A/JMJD-2 Cell Cycle Phenotypes

High overexpression of JMJD2A results in HP1 redistribution (Klose et al., 2006). Several studies have clearly demonstrated an important and highly conserved role for HP1 proteins in DNA replication (Grewal and Jia, 2007; Quivy et al., 2008; Wu et al., 2006). Based on these previous studies and the data presented here, we hypothesized that JMJD2A antagonizes HP1 proteins, resulting in faster DNA replication and S phase progression.

We first determined whether HP1 protein expression was regulated during cell cycle in a similar manner to JMJD2A. We observed that HP1γ was lowest during G1/S and S phase and highest during G2/M (Figure 6A). This pattern was reciprocal to JMJD2A (Figures 1A and 6A). HP1β also had a similar pattern during cell cycle; however, HP1α resembled the expression pattern of JMJD2A (Figure 6A).

To test the hypothesis that JMJD2A and HP1 proteins antagonize each other during S phase, all three HP1 isoforms were overexpressed in JMJD2A-overexpressing cells. S phase progression was monitored by flow cytometry and plotted based on the percentage of cells in early and late S phase 12 hr after release from nocodazole (expression levels in Figure S6A). As demonstrated earlier (Figure 1C), JMJD2A-overexpressing cells proceeded into late S phase (L) faster than control cells (Figure 6B, late S [L]; $p = 0.000064$). Overexpression of HP1α or HP1β did not alter the faster progression of JMJD2A cells. However, HP1γ overexpression completely abrogated the increased progression of JMJD2A cells into late S phase (compare JMJD2A + control to JMJD2A + HP1γ for late S [L]; $p = 0.0055$). Consistent with increased JMJD2A displacing HP1γ, knockdown of HP1γ also modestly increased progression through S phase (Figures S6B and S6C), albeit less dramatically than JMJD2A overexpression.

We then determined if the divergent N terminus, the chromodomain, or the chromo shadow domain of HP1γ was important for mediating the rescue of the JMJD2A phenotype. While overexpression of HP1γ lacking the N terminus still antagonized JMJD2A ($p = 0.0047$ with respect to JMJD2A + control), the chromodomain or the chromo shadow domain deletions were unable to compensate for JMJD2A overexpression (Figure 6B; expression levels shown in Figure S6A).

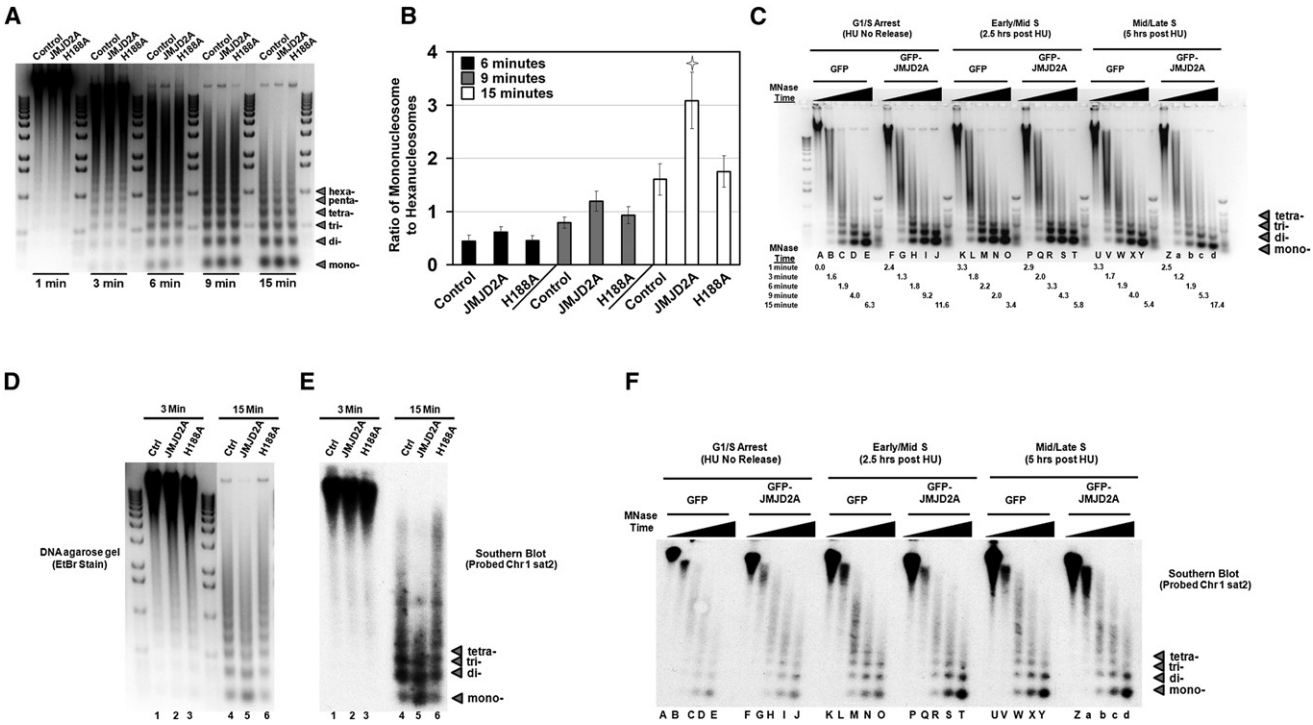

Figure 5. JMJD2A Overexpression Increases Chromatin Accessibility

(A) Representative micrococcal nuclease (MNase) digestion analysis of HEK293T cells overexpressing GFP-control or GFP-JMJD2A.

(B) Quantitation of seven biological replicates represented in (A). The percentage of mononucleosomes relative to total DNA in each lane was normalized to the amount of the highest visible nucleosome (hexanucleosome). Error bars represent the SEM. For 15 min, $p = 0.032$.

(C) MNase digestion analysis of chromatin from GFP control or GFP-JMJD2A cells during S phase (24 hr in HU [0 Hour] and washed and released for 2.5 hr [early-mid S] and 5 hr [Mid/Late S]). Black triangle represents MNase digest time titration of 1, 3, 6, 9, and 15 min. Values below the graph depict the ratio of mononucleosomes to tetranucleosomes.

(D) MNase digestion of GFP-Control, GFP-JMJD2A, or GFP-JMJD2A catalytic mutant (H188A) HEK293T cells.

(E) Chr1 sat2 is more accessible in asynchronous JMJD2A-overexpressing cells. Southern blot for Chr1 sat2 of (D).

(F) Chr1 sat2 is more accessible throughout S phase in JMJD2A-overexpressing cells. Southern Blot for Chr1 sat2 of (C).

We further verified the antagonism between HP1γ and JMJD2A during DNA replication of Chr1 sat2. HP1γ overexpression antagonizes the increased DNA replication at sat2 in JMJD2A-overexpressing cells ($p = 0.0128$), while HP1α and HP1β did not have a statistically significant impact (Figure 6C; HP1α, $p = 0.7654$; HP1β, $p = 0.1711$). Overexpression of HP1 isoforms had no impact on replication at ALU 19 (Figure S6D).

Since HP1γ and JMJD2A antagonism could be indirect, we evaluated HP1γ occupancy during S phase at Chr1 sat2 in control and JMJD2A cells. HP1γ-bound chromatin was immunoprecipitated from control and JMJD2A cells in early-mid S (released for 2.5 hr from HU). HP1γ binding was reduced upon JMJD2A overexpression (Figure 6D, $p = 0.009$). HP1γ depletion at Chr1 sat2 correlated with the increased chromatin accessibility observed in early S phase (Figure 5F). We also observed JMJD2A-dependent reduction in HP1γ binding at X cen in early-mid S phase (Figure S6E; $p = 0.007$). Consistent with the loss of HP1γ, replication of X cen was increased in early-mid S phase in JMJD2A-overexpressing cells (Figure S1G). These results demonstrate an isoform-specific antagonism between HP1γ and JMJD2A during DNA replication.

To determine if HP1γ depletion was a direct consequence of JMJD2A, we examined JMJD2A occupancy and histone methylation levels at Chr1 sat2 and X cen. In JMJD2A overexpressing cells, JMJD2A occupancy at sat2 was 2-fold higher than in control cells within the first hour of release form HU (Figure 6E) and decreased in occupancy prior to a concomitant decrease in H3K9me3 (Figure 6F; $p = 0.004$) and H3K36me3 (Figure S6H; $p = 0.003$) that coincided with the decreased binding of HP1γ. Similarly, ectopic JMJD2A bound X cen 2.5 hr after HU release (Figure S6F) and resulted in a modest decrease in H3K9me3 (Figure S6G; $p = 0.04$) without changes in H3K36me3 (Figure S6H). We did not observe significant changes in H1.4 or H1.4K26me3 at either locus 2.5 hr after HU treatment (data not shown).

We next sought to address whether this antagonism occurred in vivo. We determined whether the *C. elegans* HP1 homologs (HPL-1 and HPL-2; Schott et al., 2006) would rescue the increased DNA damage, DNA damage-induced apoptosis, and impaired DNA replication in *jmjd-2*$^{-/-}$ worms. We used both RNAi and mutant alleles for the two HP1 homologs in *C. elegans* because the *hpl-2(tm1489)* allele had pleiotropic phenotypes,

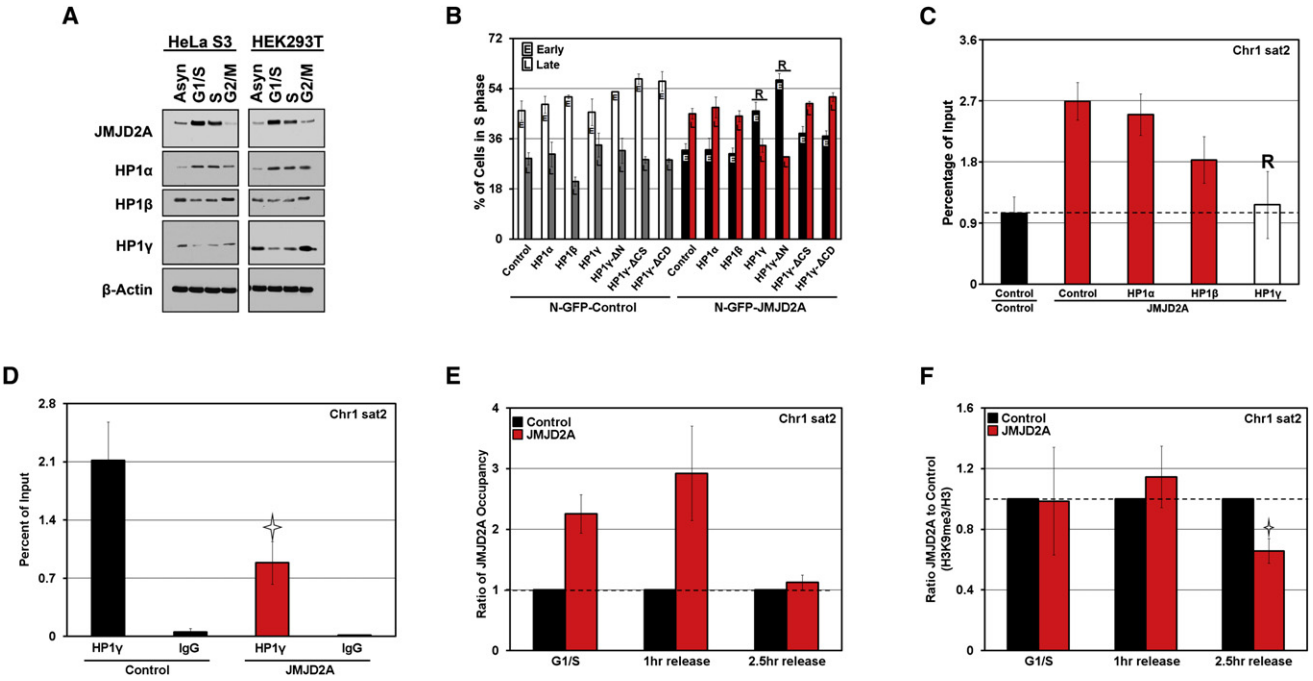

Figure 6. Functional Antagonism between JMJD2A/JMJD-2 and HP1γ/HPL-2

(A) HP1 protein levels change during cell cycle in whole-cell extracts.

(B) HP1γ antagonizes JMJD2A-dependent S phase progression. The graph depicts the percentage of cells in early (E) and late (L) S 12 hr after nocodazole release of four independent transfections and flow analyses. ΔN removes the N terminus of HP1γ before the chromodomain, ΔCS removes the chromo shadow domain, and ΔCD removes the chromodomain.

(C) HP1γ overexpression antagonizes the JMJD2A-dependent increased replication at Chr1 sat2 observed using BrdU ChIP. Graph depicts averages from at least six independent transfections.

(D) JMJD2A overexpression displaces HP1γ from chromosome 1 sat 2 in early-mid S. Cells were arrested in HU and released into fresh media for 2.5 hr prior to fixation and analysis by ChIP.

(E) JMJD2A is enriched at Chr1 sat2 within 1 hr of HU release in GFP-JMJD2A cells. Data are presented as a ratio of percent IP JMJD2A to percent IP control.

(F) H3K9me3 is depleted at Chr1 sat2 2.5 hr following HU release ($p = 0.009$). Data are presented as the ratio of percent IP of H3K9me3/percent IP of H3 in JMJD2A cells to percent IP of H3K9me3/percent IP of H3 in control cells. For all graphs, error bars represent the SEM and R represents no significant difference from control ($p > 0.05$).

including a smaller germline at 20°C (A.A. and J.R.W., unpublished data; Couteau et al., 2002). We obtained the exact same data with both RNAi and mutant alleles.

Depletion of HPL-2 had similar phenotypes to the *jmjd-2*$^{-/-}$ worms, including increased RAD-51 in the mitotic zone and decreased number of mitotic nuclei (Figures 7A and 7B). Surprisingly, HPL-2 depletion in *jmjd-2*$^{-/-}$ worms resulted in complete rescue of the increased RAD-51 foci in the mitotic and meiotic zones (Figure 7A and Figure S6I), blocked the accumulation of HU-like nuclei (Figure S6J), restored nuclei number in the mitotic zone to wild-type (Figure 7B), and rescued germline apoptosis (Figure 7C). HPL-1 depletion [*hpl-1*(*tm1624*) allele or *hpl-1* (*RNAi*)] did not rescue the increased DNA damage (Figure 7A and Figure S6I), HU-like nuclei (Figure S6J), decreased nuclei number (Figure 7B), or DNA damage-induced apoptosis in *jmjd-2*$^{-/-}$ worms (Figure 7D).

In order to better resolve the relationship between HPL-2 and JMJD-2 in DNA replication, we depleted HPL-2 from wild-type and *jmjd-2*$^{-/-}$ worms by RNAi and injected Cy3-dUTP into adult germlines. As expected, we observed decreased replication in the *jmjd-2*$^{-/-}$ mutants and wild-type worms depleted of HPL-2 (Figures 7E and 7F). However, HPL-2 depletion in the *jmjd-2*$^{-/-}$ worms rescued the impaired DNA replication (Figure 7F).

DISCUSSION

Here we demonstrate a conserved role for the JMJD2A/JMJD-2 demethylases in DNA replication. Ectopic expression of human JMJD2A promotes passage through S phase and alters replication timing, while loss of *C. elegans* JMJD-2 slowed DNA replication in the mitotic zone of the adult germline. Consistent with these observations, JMJD2A protein levels are regulated during cell cycle and are important in protecting cells from HU-induced replication stress, a role shared by JMJD-2. The increased DNA damage-induced apoptosis observed upon JMJD-2 depletion was shown to be p53 and ATR dependent but not ATM dependent, providing additional genetic data that support the role of JMJD-2 in DNA replication. Taken together, our human cell culture and *C. elegans* observations illustrate an important role for the JMJD2 family in DNA replication.

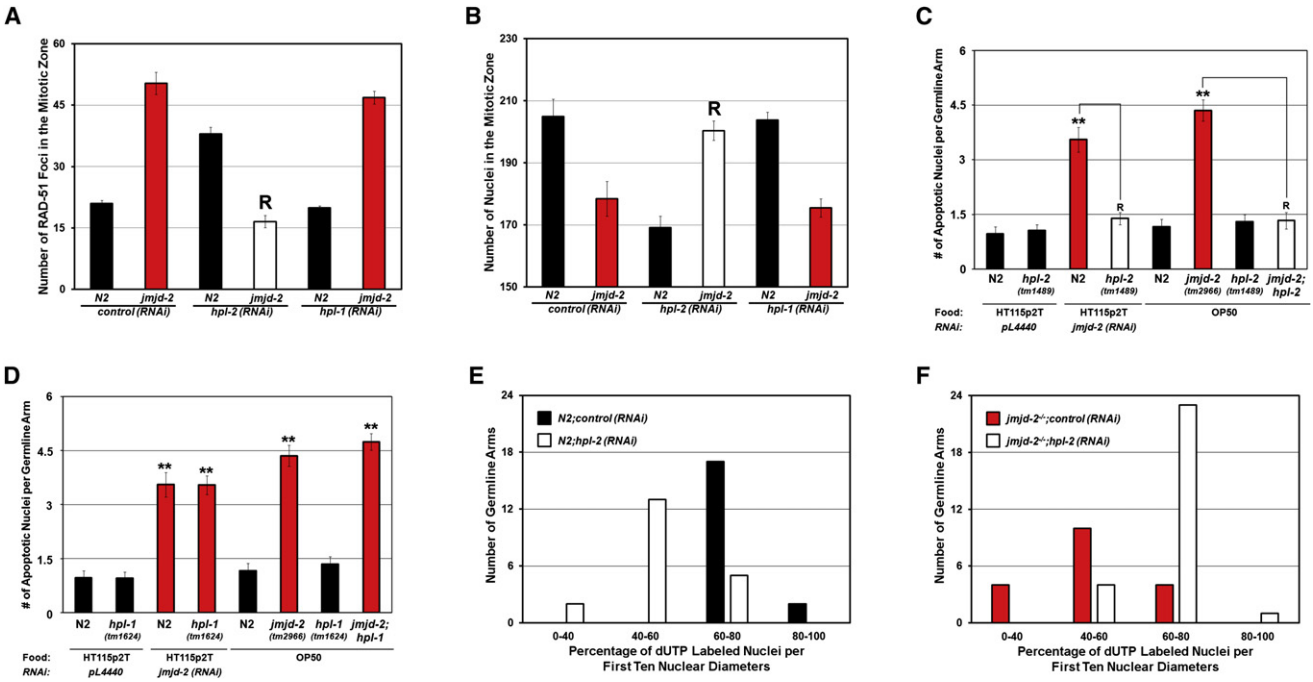

Figure 7. In Vivo Antagonism between JMJD-2 and HPL-2

(A) Depletion of HPL-2, but not HPL-1, rescues the increased RAD-51 foci observed in the mitotic zone of *jmjd-2*$^{-/-}$ animals.

(B) Depletion of HPL-2, but not HPL-1, by RNAi rescues the decreased mitotic index observed in *jmjd-2*$^{-/-}$ worms.

(C) HPL-2 depletion by either *hpl-2 (RNAi)* or *hpl-2(tm1489)* rescues the increased apoptosis observed in either *jmjd-2*$^{-/-}$ or *jmjd-2 (RNAi)*-treated worms.

(D) HPL-1 depletion by either *hpl-1 (RNAi)* or *hpl-1(tm1624)* does not rescue the increased apoptosis observed in either *jmjd-2*$^{-/-}$ or *jmjd-2 (RNAi)*-treated worms.

** indicates $p < 0.0001$. For all graphs, error bars represent the SEM of at least ten animals of each genotype. R represents no statistical difference from wild-type by two-tailed Student's t test ($p > 0.05$).

(E and F) Depletion of HPL-2 rescues the decreased replication observed in *jmjd-2*$^{-/-}$ worms. Germlines were injected with Cy3-dUTP and dissected and visualized after 4 hr (see Figure 3). (E) and (F) are graphical representations of the number of germlines with different percentages of nuclei labeled in the first ten nuclear diameters.

Interestingly, the changes in S phase progression that we observe with JMJD2A overexpression are directly paralleled by modest increases in chromatin accessibility in both asynchronous and cells progressing through S phase. Consistent with JMJD2A altering DNA replication through chromatin structure, we observed increased DNA replication at sat2 and X cen, which coincided with a decrease in HP1γ binding and increased chromatin accessibility. The increased chromatin accessibility at sat2 coincided with a change to earlier replication during S phase. We further fortified the importance of the relationship between JMJD2A/JMJD-2, chromatin structure, and DNA synthesis by demonstrating that HP1γ/HPL-2 functionally antagonized the DNA replication phenotypes observed from worm to human. Importantly, we did not observe a strong role for the other human HP1 proteins or HPL-1 in antagonizing JMJD2A/JMJD-2 function. The altered chromatin structure and antagonism observed with HP1 proteins across species suggest a highly conserved role for JMJD2A in regulating chromatin structure so that DNA synthesis has the correct spatiotemporal control.

Crosstalk between JMJD2A/JMJD-2 and HP1γ/HPL-2

Our findings describe a highly conserved model whereby JMJD2A antagonizes HP1γ to control chromatin structure and allow proper spatiotemporal timing of DNA replication (model in Figure S7). HP1 proteins could be seen as a barrier to replication initiation, or alternatively, a steric blockade to replication elongation. JMJD2A could alleviate this by removal of H3K9/36me3, allowing proper spatiotemporal control of replication. Consistent with this model, JMJD2A overexpression resulted in a modestly more open chromatin conformation, decreased HP1γ occupancy, decreased H3K9me3, and increased replication of Chr1 sat2 and a region near the X centromere.

HP1γ required both the chromodomain and chromo shadow domain to antagonize JMJD2A-dependent S phase progression, supporting the model that HP1γ requires the ability to bind methyl modifications and interact with other chromatin regulators to antagonize JMJD2A (Kwon and Workman, 2008). While HP1γ binding could be controlled independently of histone modifications, the changes to H3K9me3 at sat2 are likely responsible for the reduction in HP1γ occupancy. While it is possible nonhistone substrates may be important, it seems likely given the importance of the methyltransferases in yeast, mouse, and human systems that at least part of the role of JMJD2A/JMJD-2 in S phase progression is through demethylation of H3K9me3.

Loss of JMJD-2 in *C. elegans* slowed DNA replication. In this scenario, JMJD-2 loss would result in an inability to disrupt the

HP1 steric blockade so that replication initiation and/or elongation are impaired (model in Figure S7). As predicted from the model, HPL-2 depletion rescued the defects in *jmjd-2*$^{-/-}$ worms. Alternatively, loss of *jmjd-2* could result in increased histone methylation, resulting in spread and dilution of HPL-2 to additional regions not normally controlled by HPL-2.

Interestingly, loss of HPL-2 by itself led to increased RAD-51 foci in the mitotic zone, fewer mitotic nuclei, and defects in replication. Thus, it was surprising that HPL-2 depletion rescued the same defects in *jmjd-2*$^{-/-}$ animals. Our results suggest that controlling the levels and distribution of HPL-2 is crucial for germline nuclei proliferation. HPL-2 loss could cause replication defects through at least two mechanisms: (1) HPL-2 loss removes constraints on chromatin, resulting in inappropriate early replication, which could trigger ATR checkpoint resulting in overall loss of replication efficiency. (2) Loss of HPL-2 could result in spreading and mislocalization of HPL-1, resulting in inappropriate regulation of replication. These observations suggest that there is an intricate antagonistic relationship between the demethylase and specific HP1 homologs.

Relationship between HP1γ and HPL-2

We observed less DNA replication in young adults treated with both *hpl-2 (RNAi)* or JMJD-2 depletion; however, codepletion restored the worms to wild-type levels. The specific role of HPL-2 in the mitotic zone could reflect changes in chromatin structure, as well as transcriptional changes. Both HPL-2 and HP1γ are able to rescue the JMJD-2 and JMJD2A phenotypes, respectively. These data suggest that HPL-2 may in fact be a functional homolog to HP1γ. Although sequence homology does not resolve this relationship, our functional observations across species raise this interesting possibility.

JMJD2A, Chromatin Structure, and DNA Replication

Our results highlight the importance of controlling chromatin structure during replication and implicate JMJD2 histone demethylases as contributors to this regulation. MacAlpine et al. recently demonstrated that increasing the number of potential origins within a region correlates with earlier replication timing (MacAlpine et al., 2010). Consistent with changes in initiation, we observed increased production of ssDNA, indicative of increased replication forks in JMJD2A-overexpressing cells. This suggests that JMJD2A might be creating more favorable chromatin conditions for initiation of replication. Furthermore, JMJD2A overexpression resulted in earlier replication of Chr1 sat2, demonstrating the ability of JMJD2A to impact replication timing. Our results do not exclude the possibility that JMJD2A is also contributing to changes in replication by altering elongation rates.

The ability of a chromatin modifier like JMJD2A to alter the modification state and the underlying structure could have a direct impact on the plasticity observed within specific genomic regions. JMJD2A and HP1γ could be important regulators of epigenetic states required for maintaining replication timing or specifying borders of replication domains.

We would predict that additional chromatin modifiers (e.g., histone demethylases and histone methyltransferases) will be able to alter both chromatin state and cell cycle progression. Indeed, the methyltransferase Dot1 regulates cell cycle genes through H3K79me2 and is required for efficient entry into S phase (Schulze et al., 2009). Our data strongly suggest that chromatin modifiers can also impact cell cycle through chromatin structure. However, these two effects do not have to be mutually exclusive. There is a strong possibility that chromatin regulators will influence both aspects, allowing for a tighter level of control of cell cycle progression. These results suggest that cells and perhaps individual origins must proceed through a chromatin checkpoint. Understanding what factors establish, read, maintain, and overcome this checkpoint will be critical to advance our knowledge of proper spatial and temporal control of replication.

EXPERIMENTAL PROCEDURES

Cell Culture and Synchronization

HEK293T and HeLa S cells were grown in DMEM supplemented with 10% heat-inactivated fetal bovine serum, 50 I.U. per ml penicillin, 50 μg per ml streptomycin, and 2 mM L-glutamine. Stable cell lines were periodically reselected in 3 ug/ml puromycin or by FACS to select GFP-positive cells. All experiments were performed with cells at least one passage postpuromycin treatment. Cells were synchronized by treatment with 1 mM HU (Sigma) for 24 hr or 50 ng/ml nocodazole (Sigma) for 10 hr. G2/M-arrested cells were collecting by mitotic shakeoff. To release arrested cells, cells were washed once with media and supplied fresh media.

Generation of Stable Cell Lines

Retrovirus was generated in Phoenix A cells 48 hr posttransfection. Cells were infected twice and allowed to recover 24–48 hr prior to selection. Cells were selected twice with 4 ug/ml puromycin for 48–72 hr with a 48 hr recovery period between puromycin treatments. Stable lines were verified by RT-qPCR and western analysis. Each cell line was created at least two or more times and used in the experiments described above. Subsequent selections were performed by sorting for GFP-positive cells.

Cell Growth Curves

Cells were plated in triplicate in six-well dishes at 4×10^4 cells per well. For growth curves, the cells were counted 24, 48, and 72 hr after plating. Cells were harvested and stained with trypan blue, and live cells were manually counted using a hemocytometer. The number of live cells counted at 24 hr was set as a relative population of 1. The cell number at 48 and 72 hr was normalized to this value to generate relative population. For HU release analysis, cells were treated with 1 mM HU on the day after plating. Twenty-four hours after addition of HU (day 0), cells were released and counted at 0, 24, 48, and 72 hr. The relative populations were calculated by normalizing to the number of live cells at day zero.

Analysis of Single-Stranded DNA during S Phase

1×10^6 cells were seeded in a 10 cm dish for 24 hr prior to labeling with Cell Proliferation and Labeling Reagent (GE Healthcare) for 24 hr. Cells were supplied fresh media and arrested in nocodazole for 10 hr. Cells were released and harvested in RIPA buffer at the indicated time points. Experiment was performed with minor modifications from (Jasencakova et al., 2010). DNA was slot blotted and analyzed for BrdU (BD Biosciences). Film was scanned and analyzed using ImageJ V1.43 (NIH). For each time point the ratio of native/denatured BrdU signal was calculated.

BrdU DNA Immunoprecipitation

1×10^6 cells were seeded in a 10 cm dish. Thirty-six to forty-eight hours after seeding, cells were treated for 1 hour with Cell Proliferation and Labeling Reagent (GE Healthcare). Cells were collected and BrdU ChIP was performed as described in Hansen et al. (2010). The complete method can be found in the Supplemental Information. Chr1 sat2 primers are identical to those used in

(Zeng et al., 2009). X cen primers amplify a 96 bp amplicon at 61,569 KB from the left arm of the chromosome in the region designated as the centromere on the UCSC genome browser using the NCBI36.3/hg18 build. This region lies within a 2 KB repeat encompassing approximately 36 KB.

Chromatin Immunoprecipitation

1.5×10^6 cells were seeded in four 15 cm dishes. Thirty-six hours after seeding, cells were treated with 1 mM HU. Twenty-four hours after treatment, cells were released for analysis of S phase. Chromatin immunoprecipitation (ChIP) experiments were done as described earlier with slight modifications (Shi et al., 2003). A complete protocol can be found in the Supplemental Information. For JMJD2A, all IPs were above 0.2% of input. For histones and histone modifications, all IPs were greater than 3% of input.

Flow Cytometry

Complete methods can be found in the Supplemental Information. Sorting of live cells for replication timing was performed as in Hansen et al. (2010).

Western Blots

Western blots were performed according to Whetstine et al. (2006). A complete antibody list is in the Supplemental Information.

Micrococcal Nuclease Assay

2×10^6 cells were seeded in a 15 cm dish 24 hr prior to the experiment. Complete methods can be found in the Supplemental Information. Images were captured on a GelDoc XR (Bio-Rad) using Quantity One software. Exported JPEGs were quantitated using ImageJ v1.43 (NIH).

C. elegans Strain Maintenance and RNAi Knockdown

Worms were cultured at 20°C on NGM plates seeded with OP50 as previously described (Brenner, 1974). For all experiments, L1 larvae were synchronized by hypochlorite treatment of gravid adults and allowed to grow for 62 hr before analysis. A complete list of strains is in the Supplemental Information. RNAi knockdown of *C. elegans* genes was as previously described (Whetstine et al., 2006).

Dissection, DAPI Staining, and Antibody Staining of the *C. elegans* Germline

Dissection, DAPI staining, and antibody staining of *C. elegans* germlines were carried out largely as previously described (Colaiacovo et al., 2003; Whetstine et al., 2006). Optical sections were collected at 0.2 or 0.5 μm intervals using an ix81 spinning disc confocal microscope (Olympus). Images were acquired and analyzed using Slidebook 5.0.0.1.

Cy3- and Alexa 488-dUTP Analysis of the *C. elegans* Germline

Injections were done on animals 62 hr post-L1 release grown on either NGM plates seeded with OP50 or RNAi plates seeded with the appropriate RNAi food source at 20°C. Cy3-dUTP (GE) was injected at a concentration of 1 pmol/μl into young adult *C. elegans* germ lines as previously described (Jaramillo-Lambert et al., 2007). Complete methods can be found in the Supplemental Information.

Analysis of Hydroxyurea Sensitivity of *C. elegans* Embryos

Fifteen synchronized young adult animals were seeded to five NGM plates containing the indicated concentration of HU (Sigma-Aldrich) and 10 μl of concentrated OP50 or RNAi food for 13 hr at 20°C. Eggs were quantified and embryonic lethality was scored 20 hr later. All experiments were done in triplicate.

Quantitative Analysis of *C. elegans* Germline Apoptosis

Scoring and analysis of germ line apoptosis was done as previously described (Whetstine et al., 2006).

SUPPLEMENTAL INFORMATION

Supplemental Information includes seven figures, Supplemental Experimental Procedures, and Supplemental References and can be found with this article at doi:10.1016/j.molcel.2010.11.008.

ACKNOWLEDGMENTS

We are grateful to Ravi Mylvaganam and the MGH Flow Cytometry core for assistance with the FACS analysis. We would like to thank Sigrid Jacobshagen for technical assistance and Othon Iliopoulos for helpful discussions and comments on the manuscript. We thank Jane Hubbard for suggestions and technical advice regarding mitotic germline nuclei. We thank Steve Smale for providing antibodies to HP1α and HP1β, and Adriana La Volpe for providing antibody to RAD-51. We thank Dr. Shohei Mitani of the National Bioresource Project for the *tm2966* deletion allele and the CGC for additional *C. elegans* mutant strains. This work was supported by funding to J.R.W. from the Ellison Medical Foundation, Milton Fund, Astra Zeneca MGH Alliance, and the Howard Goodman Fellowship. J.C.B. is a Fellow of The Jane Coffin Childs Memorial Fund for Medical Research. This investigation has been aided by a grant from The Jane Coffin Childs Memorial Fund for Medical Research.

Received: March 6, 2010
Revised: June 8, 2010
Accepted: September 10, 2010
Published: December 9, 2010

REFERENCES

Bannister, A.J., Zegerman, P., Partridge, J.F., Miska, E.A., Thomas, J.O., Allshire, R.C., and Kouzarides, T. (2001). Selective recognition of methylated lysine 9 on histone H3 by the HP1 chromo domain. Nature *410*, 120–124.

Bernstein, B.E., Meissner, A., and Lander, E.S. (2007). The mammalian epigenome. Cell *128*, 669–681.

Biswas, D., Takahata, S., Xin, H., Dutta-Biswas, R., Yu, Y., Formosa, T., and Stillman, D.J. (2008). A role for Chd1 and Set2 in negatively regulating DNA replication in Saccharomyces cerevisiae. Genetics *178*, 649–659.

Brenner, S. (1974). The genetics of Caenorhabditis elegans. Genetics *77*, 71–94.

Chen, E.S., Zhang, K., Nicolas, E., Cam, H.P., Zofall, M., and Grewal, S.I. (2008). Cell cycle control of centromeric repeat transcription and heterochromatin assembly. Nature *451*, 734–737.

Cimbora, D.M., Schubeler, D., Reik, A., Hamilton, J., Francastel, C., Epner, E.M., and Groudine, M. (2000). Long-distance control of origin choice and replication timing in the human beta-globin locus are independent of the locus control region. Mol. Cell. Biol. *20*, 5581–5591.

Cloos, P.A., Christensen, J., Agger, K., and Helin, K. (2008). Erasing the methyl mark: histone demethylases at the center of cellular differentiation and disease. Genes Dev. *22*, 1115–1140.

Colaiacovo, M.P., MacQueen, A.J., Martinez-Perez, E., McDonald, K., Adamo, A., La Volpe, A., and Villeneuve, A.M. (2003). Synaptonemal complex assembly in *C. elegans* is dispensable for loading strand-exchange proteins but critical for proper completion of recombination. Dev. Cell *5*, 463–474.

Couteau, F., Guerry, F., Muller, F., and Palladino, F. (2002). A heterochromatin protein 1 homologue in Caenorhabditis elegans acts in germline and vulval development. EMBO Rep. *3*, 235–241.

Czvitkovich, S., Sauer, S., Peters, A.H., Deiner, E., Wolf, A., Laible, G., Opravil, S., Beug, H., and Jenuwein, T. (2001). Over-expression of the SUV39H1 histone methyltransferase induces altered proliferation and differentiation in transgenic mice. Mech. Dev. *107*, 141–153.

Daujat, S., Zeissler, U., Waldmann, T., Happel, N., and Schneider, R. (2005). HP1 binds specifically to Lys26-methylated histone H1.4, whereas simultaneous Ser27 phosphorylation blocks HP1 binding. J. Biol. Chem. *280*, 38090–38095.

Dohke, K., Miyazaki, S., Tanaka, K., Urano, T., Grewal, S.I., and Murakami, Y. (2008). Fission yeast chromatin assembly factor 1 assists in the replication-coupled maintenance of heterochromatin. Genes Cells *13*, 1027–1043.

Fodor, B.D., Kubicek, S., Yonezawa, M., O'Sullivan, R.J., Sengupta, R., Perez-Burgos, L., Opravil, S., Mechtler, K., Schotta, G., and Jenuwein, T. (2006). Jmjd2b antagonizes H3K9 trimethylation at pericentric heterochromatin in mammalian cells. Genes Dev. *20*, 1557–1562.

Fraga, M.F., and Esteller, M. (2005). Towards the human cancer epigenome: a first draft of histone modifications. Cell Cycle *4*, 1377–1381.

Garcia-Muse, T., and Boulton, S.J. (2005). Distinct modes of ATR activation after replication stress and DNA double-strand breaks in Caenorhabditis elegans. EMBO J. *24*, 4345–4355.

Grewal, S.I., and Jia, S. (2007). Heterochromatin revisited. Nat. Rev. Genet. *8*, 35–46.

Hansen, R.S., Thomas, S., Sandstrom, R., Canfield, T.K., Thurman, R.E., Weaver, M., Dorschner, M.O., Gartler, S.M., and Stamatoyannopoulos, J.A. (2010). Sequencing newly replicated DNA reveals widespread plasticity in human replication timing. Proc. Natl. Acad. Sci. USA *107*, 139–144.

Hayashi, M.T., Takahashi, T.S., Nakagawa, T., Nakayama, J., and Masukata, H. (2009). The heterochromatin protein Swi6/HP1 activates replication origins at the pericentromeric region and silent mating-type locus. Nat. Cell Biol. *11*, 357–362.

Huang, D.W., Fanti, L., Pak, D.T., Botchan, M.R., Pimpinelli, S., and Kellum, R. (1998). Distinct cytoplasmic and nuclear fractions of Drosophila heterochromatin protein 1: their phosphorylation levels and associations with origin recognition complex proteins. J. Cell Biol. *142*, 307–318.

Jaramillo-Lambert, A., Ellefson, M., Villeneuve, A.M., and Engebrecht, J. (2007). Differential timing of S phases, X chromosome replication, and meiotic prophase in the C. elegans germ line. Dev. Biol. *308*, 206–221.

Jasencakova, Z., Scharf, A.N., Ask, K., Corpet, A., Imhof, A., Almouzni, G., and Groth, A. (2010). Replication stress interferes with histone recycling and predeposition marking of new histones. Mol. Cell *37*, 736–743.

Karnani, N., Taylor, C.M., Malhotra, A., and Dutta, A. (2010). Genomic study of replication initiation in human chromosomes reveals the influence of transcription regulation and chromatin structure on origin selection. Mol. Biol. Cell *21*, 393–404.

Kim, H.S., Rhee, D.K., and Jang, Y.K. (2008). Methylations of histone H3 lysine 9 and lysine 36 are functionally linked to DNA replication checkpoint control in fission yeast. Biochem. Biophys. Res. Commun. *368*, 419–425.

Klose, R.J., Yamane, K., Bae, Y., Zhang, D., Erdjument-Bromage, H., Tempst, P., Wong, J., and Zhang, Y. (2006). The transcriptional repressor JHDM3A demethylates trimethyl histone H3 lysine 9 and lysine 36. Nature *442*, 312–316.

Kwon, S.H., and Workman, J.L. (2008). The heterochromatin protein 1 (HP1) family: put away a bias toward HP1. Mol. Cells *26*, 217–227.

Lachner, M., O'Carroll, D., Rea, S., Mechtler, K., and Jenuwein, T. (2001). Methylation of histone H3 lysine 9 creates a binding site for HP1 proteins. Nature *410*, 116–120.

Lan, F., Nottke, A.C., and Shi, Y. (2008). Mechanisms involved in the regulation of histone lysine demethylases. Curr. Opin. Cell Biol. *20*, 316–325.

MacAlpine, D.M., Rodriguez, H.K., and Bell, S.P. (2004). Coordination of replication and transcription along a Drosophila chromosome. Genes Dev. *18*, 3094–3105.

MacAlpine, H.K., Gordan, R., Powell, S.K., Hartemink, A.J., and MacAlpine, D.M. (2010). Drosophila ORC localizes to open chromatin and marks sites of cohesin complex loading. Genome Res. *20*, 201–211.

Maison, C., Bailly, D., Peters, A.H., Quivy, J.P., Roche, D., Taddei, A., Lachner, M., Jenuwein, T., and Almouzni, G. (2002). Higher-order structure in pericentric heterochromatin involves a distinct pattern of histone modification and an RNA component. Nat. Genet. *30*, 329–334.

Mendez, J. (2009). Temporal regulation of DNA replication in mammalian cells. Crit. Rev. Biochem. Mol. Biol. *44*, 343–351.

Moss, T.J., and Wallrath, L.L. (2007). Connections between epigenetic gene silencing and human disease. Mutat. Res. *618*, 163–174.

Nakayama, J., Rice, J.C., Strahl, B.D., Allis, C.D., and Grewal, S.I. (2001). Role of histone H3 lysine 9 methylation in epigenetic control of heterochromatin assembly. Science *292*, 110–113.

Quivy, J.P., Gerard, A., Cook, A.J., Roche, D., and Almouzni, G. (2008). The HP1-p150/CAF-1 interaction is required for pericentric heterochromatin replication and S-phase progression in mouse cells. Nat. Struct. Mol. Biol. *15*, 972–979.

Schott, S., Coustham, V., Simonet, T., Bedet, C., and Palladino, F. (2006). Unique and redundant functions of C. elegans HP1 proteins in post-embryonic development. Dev. Biol. *298*, 176–187.

Schubeler, D., Francastel, C., Cimbora, D.M., Reik, A., Martin, D.I., and Groudine, M. (2000). Nuclear localization and histone acetylation: a pathway for chromatin opening and transcriptional activation of the human beta-globin locus. Genes Dev. *14*, 940–950.

Schulze, J.M., Jackson, J., Nakanishi, S., Gardner, J.M., Hentrich, T., Haug, J., Johnston, M., Jaspersen, S.L., Kobor, M.S., and Shilatifard, A. (2009). Linking cell cycle to histone modifications: SBF and H2B monoubiquitination machinery and cell-cycle regulation of H3K79 dimethylation. Mol. Cell *35*, 626–641.

Shi, Y., Sawada, J., Sui, G., Affar el, B., Whetstine, J.R., Lan, F., Ogawa, H., Luke, M.P., Nakatani, Y., and Shi, Y. (2003). Coordinated histone modifications mediated by a CtBP co-repressor complex. Nature *422*, 735–738.

Stergiou, L., Doukoumetzidis, K., Sendoel, A., and Hengartner, M.O. (2007). The nucleotide excision repair pathway is required for UV-C-induced apoptosis in Caenorhabditis elegans. Cell Death Differ. *14*, 1129–1138.

Trojer, P., Zhang, J., Yonezawa, M., Schmidt, A., Zheng, H., Jenuwein, T., and Reinberg, D. (2009). Dynamic histone H1 isotype 4 methylation and demethylation by histone lysine methyltransferase G9a/KMT1C and the Jumonji domain-containing JMJD2/KDM4 proteins. J. Biol. Chem. *284*, 8395–8405.

Vakoc, C.R., Mandat, S.A., Olenchock, B.A., and Blobel, G.A. (2005). Histone H3 lysine 9 methylation and HP1gamma are associated with transcription elongation through mammalian chromatin. Mol. Cell *19*, 381–391.

Weidtkamp-Peters, S., Rahn, H.P., Cardoso, M.C., and Hemmerich, P. (2006). Replication of centromeric heterochromatin in mouse fibroblasts takes place in early, middle, and late S phase. Histochem. Cell Biol. *125*, 91–102.

Whetstine, J.R., Nottke, A., Lan, F., Huarte, M., Smolikov, S., Chen, Z., Spooner, E., Li, E., Zhang, G., Colaiacovo, M., and Shi, Y. (2006). Reversal of histone lysine trimethylation by the JMJD2 family of histone demethylases. Cell *125*, 467–481.

Wu, R., Terry, A.V., Singh, P.B., and Gilbert, D.M. (2005). Differential subnuclear localization and replication timing of histone H3 lysine 9 methylation states. Mol. Biol. Cell *16*, 2872–2881.

Wu, R., Singh, P.B., and Gilbert, D.M. (2006). Uncoupling global and fine-tuning replication timing determinants for mouse pericentric heterochromatin. J. Cell Biol. *174*, 185–194.

Zeng, W., de Greef, J.C., Chen, Y.Y., Chien, R., Kong, X., Gregson, H.C., Winokur, S.T., Pyle, A., Robertson, K.D., Schmiesing, J.A., et al. (2009). Specific loss of histone H3 lysine 9 trimethylation and HP1gamma/cohesin binding at D4Z4 repeats is associated with facioscapulohumeral dystrophy (FSHD). PLoS Genet. *5*, e1000559. 10.1371/journal.pgen.1000559.